Transactions on Computer Science and Intelligent Systems Research
ISSN: 2960-1800, eISSN: 2960-2238 | Volume 7
TPCEE 2024

Advanced Optical Efficiency Analysis of Tower Solar Heliostat Fields based on Monte Carlo Ray Tracing and Analytic Geometry method

Di Wang[#,*], Qingyuan Cao[#], Yujun Liu[#], Shan Ma[#]

Shool of Mathematics and Statistics, Lanzhou University, Lanzhou, China, 730000

* Corresponding Author Email: wangdi2019@lzu.edu.cn

#These authors contributed equally.

Abstract. Solar thermal tower power is an innovative technology that uses a field of heliostats to convert solar energy into electricity. The ability to accurately compute the optical efficiency and thermal power output is a crucial aspect of effectively employing this technology, subsequently enhancing power generation efficiency through strategies such as optimizing the distribution of the heliostat field. An innovative approach for calculating the annual mean optical efficiency, annual mean output thermal power will be presented in this paper. To calculate the related parameters, a spatial Cartesian coordinate system will be established in this paper by utilizing conventional analytical geometry techniques. This methodology explicitly provides the trigonometric functions for diverse angles, thereby eliminating inaccuracies linked to approximations, guaranteeing that subsequent algorithms deal with the minimal number of variables necessary to achieve a more precise fitting outcome. Regarding the shadow occlusion efficiency, basic analytical geometry will be adopted to simulate the positional relationships and solar reflection angles of the heliostats. This method enables us to compute an annual mean shadow occlusion efficiency of approximately 0.8412. As for the collector truncation efficiency, this paper has developed a ray tracing model based on Monte Carlo random sampling. This model decomposes the solar light cone into discrete rays, which allows us to use the simulation model to assess whether the rays impact the collector. By integrating the energy carried by rays that meet the requirements, this paper quantifies the energy received by the collector, resulting in an annual mean truncation efficiency of 0.8723.

Keywords: Monte Carlo ray tracing; Basic Analytic Geometry; Shadow blocking theory; Heliostats field.

1. Introduction

Concentrated Solar Power (CSP) is considered an environmentally friendly and low-carbon energy technology. Owing to the reliable and effective characteristics of solar power, CSP is highly esteemed by governmental bodies and the scientific community as a particularly promising form of renewable energy technology. A standard solar thermal power plant consists of three primary elements: a heat collector, a heliostat field, and an energy conversion mechanism. During operation, the control system adjusts the orientation of the heliostats in response to the sun's position, ensuring precise concentration of sunlight onto the collector. Subsequently, the energy conversion device aids in transforming solar energy into thermal energy and then into electrical energy [1]. Thus, enhancing CSP design for solar energy aims to reduce losses and maximize energy utilization, which is practically important.

CSP can be categorized into four main types: parabolic trough, central receiver system (CRS), linear Fresnel, and dish Stirling [2], based on the approaches to concentrating solar radiation and the heat collector technologies employed. The first large-scale CSP plant, employing a parabolic trough design, was established in Egypt in 1913[3]. In the 1960s, as the importance of photovoltaics in space programs gained recognition, the first linear Fresnel heliostat array was constructed by Francia in 1961[4]. Subsequently, in the latter part of the same decade, Francia also developed a prototype for a CRS in Genoa in 1968[5]. Dish Stirling solar thermal power generation began much later, despite

the initial proposal of the Stirling engine by Scottish inventor Robert Stirling in 1816 [6]. It was only in 2000 that dish Stirling energy systems started being implemented in the USA [7]. PTC is considered the top choice among CSP technologies because of its fast technological progress, cost efficiency, and high performance [8][9][10], making it the preferred option for those considering setting up photothermal fields.

A general method for calculating the annual mean optical efficiency, annual mean output thermal power, and annual mean output thermal power per unit mirror area of CSP will be provided in this paper. Calculations of the parameters pertaining to optical efficiency within a spatial Cartesian coordinate system will be performed in this paper by utilizing conventional analytical geometry techniques. This methodology explicitly provides the trigonometric functions for diverse angles, thereby eliminating inaccuracies linked to approximations and sidestepping the confusion in physical interpretation stemming from angle substitutions. Through the employment of the most basic mathematical functions inherent in the spatial Cartesian coordinate system for the computation of parameters associated with optical efficiency, the precision during the initial phase of processing parameters in the optimization of CSP will be bolstered in this paper. This approach of direct computation diminishes potential errors in each stage of assumption, guaranteeing that subsequent algorithms deal with the minimal number of variables necessary to achieve a more precise fitting outcome.

2. Establishment and solution of the model

The data utilized in this paper were sourced from http://www.mcm.edu.cn/html_cn/node/c74d72127066f510a5723a94b5323a26.html.

For calculating the annual mean optical efficiency, annual mean output thermal power, and annual mean output thermal power per unit mirror area of CSP, it is necessary to address I the shadow occlusion efficiency, cosine efficiency, and the interception efficiency of heat absorber within the optical efficiency of the heliostat; II the direct normal irradiance to subsequently determine the power output of the heliostat field.

The solution process of I involves: To solve for the shadow occlusion efficiency, an equation of the mirror surface is first established within the field's coordinate system, leading to the derivation of the shadowed area equation. Under specified constraints, the shadowed area is obtained. To determine the cosine efficiency, the relationship between the angle's cosine value formed by the incident light on the mirror surface and the normal will be established in this paper, transforming the indirect method of calculating cosine losses into a direct computation of cosine efficiency. When solving for the interception efficiency of heat absorber, the Monte Carlo ray-tracing method is used to determine the energy flux density function on the heat absorber surface, simulating the energy flow losses on the absorption surface.

The solution process of II involves: Utilizing the shadow occlusion efficiency derived in I to obtain the effective light-collecting area of the heliostat. Integrating the existing data provided in the problem statement and substituting into the formula yields the thermal power output of the heliostat field. The main assumptions used in this paper are as follows:

•Assumption one: the central point of the heliostat mirror is located on the central axis of the base, with the center of the mirror coinciding vertically with the support point of the mirror.

•Assumption two: the sunlight is parallel when calculating the shadow occlusion area and conical when illuminating the tower.

• Assumption three: the energy carried by the sunlight at each point on the mirror surface is uniform.

• Assumption four: the heliostat field is an ideal horizontal plane, with all heliostats having the same column height, conforming to the same rectangular specification, and using altitude-angle and pitch-angle tracking methods.

• Assumption five: the computations are carried out for a clear day with abundant sunshine, thereby overlooking the influence of meteorological conditions on the optical performance of the heliostat array.

2.1. Establishment of a heliostat field coordinate system

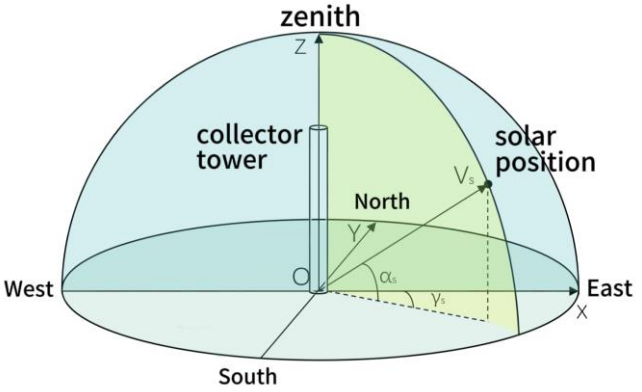

Figure 1. The three-dimensional coordinate system of the heliostat field

In solar tower power stations, the heliostat fields are generally arranged circumferentially around the central receiver tower. A spatial Cartesian coordinate system with the receiver tower as the coordinate origin can represent this layout, applicable to both circular radiation-type heliostat fields and square crop-type fields. In this paper, a horizontal coordinate system will be used to aid in describing the positions of the sun and the heliostats. As depicted in Figure 1, the coordinate origin is set at the intersection of the central axis of the receiver tower with the plane of the heliostat field. The origin O is specifically defined as the geometric center of the tower base. The positive X axis is directed eastward, the positive Y axis is oriented northward, and the positive Z axis is aligned with the zenith. This establishes a three-dimensional Cartesian coordinate system for the field based on the data provided in the question, calculations reveal that the heliostat field is distributed in an elliptical radiation pattern [11].

As depicted in Figure 2 and according to the data presented in the problem statement, computations suggest that the heliostat field under consideration is arranged in an elliptical radiation pattern.

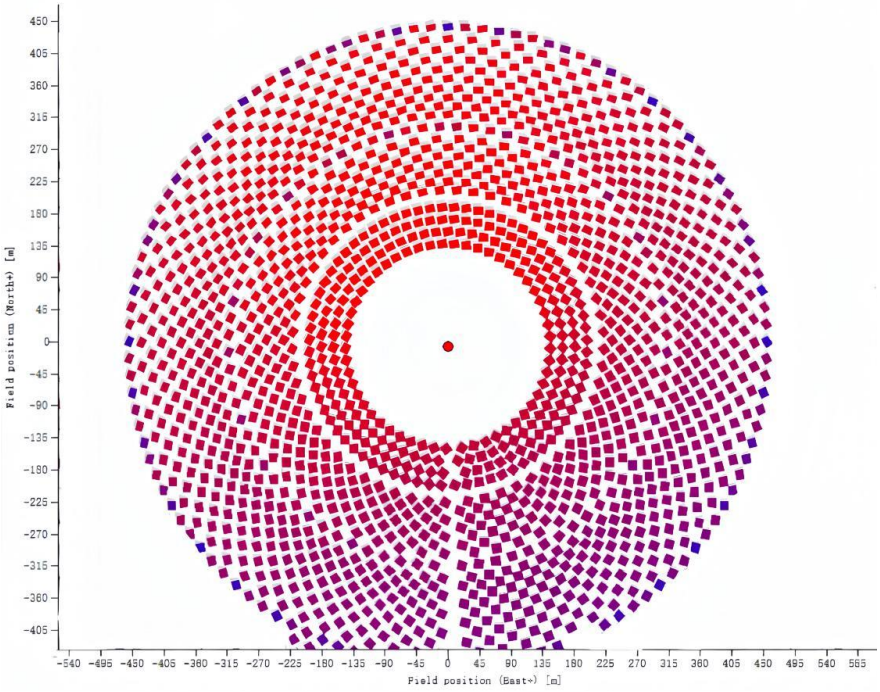

Figure 2. Scatter plot of heliostat from above

In this case, one can ascertain the values of sine α_s and cosine γ_s by using the principles of sine and cosine theorems. Here, α_s represents the sun's location elevation angle, whereas γ_s indicates the sun's position azimuth angle. Both α_s and γ_s are quantified in radians.

The irradiance of direct normal radiation (DNI) in kilowatts per square meter (kW/m^2) pertains to the Earth's surface that is perpendicular to the incoming sunlight. The solar energy from radiation that is received within a certain area over a specific period can be estimated by employing the subsequent mathematical expressions (1)-(4):

$$DNI = G_0\left[a + bexp\left(\frac{-c}{sin\alpha_s}\right)\right] \tag{1}$$

$$a = 0.4237 - 0.00821(6 - H)^2 \tag{2}$$

$$b = 0.5055 + 0.00595(6.5 - H)^2 \tag{3}$$

$$c = 0.2711 + 0.01858(2.5 - H)^2 \tag{4}$$

Suppose $G_0 = 1.366\text{k}W/m^2$, refers to solar constant, Where H is the altitude above sea level (Unit: km).

E_{field} represents output thermal power of heliostat field. It can be estimated from mathematical expression (5):

$$E_{field} = DNI\sum_i^N A_i\eta_i \tag{5}$$

Where N is the total number of heliostats (unit: face); A_i is the lighting area of the i-th heliostat (unit: m2); η_i is the optical efficiency of the i-th mirror.

2.2. The Calculation of Optical Efficiency

Sunlight is transmitted to the surface of the collector or the mouth of the heat absorbing cavity after a reflection by the heliostat field, then sunlight characterized by a low energy density undergoes concentration by the heliostat field into high-energy-density beams, which then undergo conversion from solar radiative energy to thermal energy at the receiver surface. The optical efficiency of the heliostat field is characterized as the ratio of energy captured by the receiver to the overall energy of the incident sunlight. The effectiveness of a heliostat array is impacted by a range of variables, including the solar position, heliostat layout, and atmospheric circumstances. These serve as crucial parameters in the assessment of the focusing capacity of a heliostat field [1]. The optical efficiency of a heliostat field is composed of five fundamental elements: cosine efficiency η_{cos}, atmospheric transmittance η_{at}, shadow occlusion efficiency η_{sb}, receiver truncation efficiency η_{trunc}, mirror reflectivity η_{ref}. During any given time, the immediate optical efficiency of a heliostat can be calculated by multiplying these five components:

$$\eta = \eta_{ref}\eta_{at}\eta_{cos}\eta_{sb}\eta_{trunc} \tag{6}$$

2.2.1. Mirror reflectivity

In the formula (6), the reflectivity η_{ref} of a heliostat mirror is primarily dependent on the material used. Typically, the reflectance values of glass mirrors typically fall within the range of 0.93 to 0.94, and they are known to have a standard operational longevity of 20 to 25 years [12]. However, prolonged exposure to sunlight can reduce the reflectivity due to aging of the mirror surface. Additionally, environmental elements such as frost, rain, and snow can accumulate dust and impurities on the mirror surface, not only diminishing its reflectivity but also causing light scattering. These factors impact the focusing performance. The maintenance and cleanliness of the mirror

surface are also crucial to its functionality. Based on the provided data, the reflectivity at 0.92 will be adopted in this paper.

2.2.2. Atmospheric transmittance

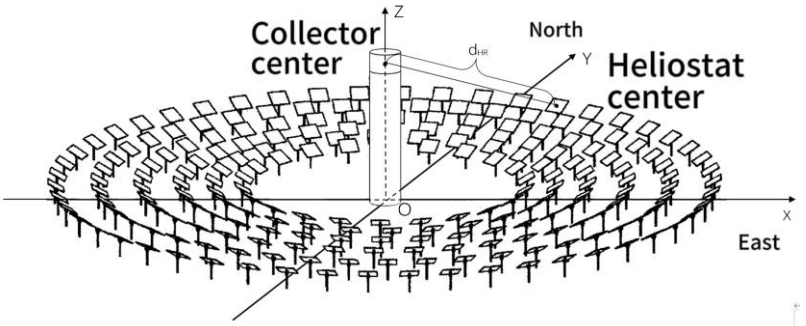

Figure 3. Schematic diagram of heliostat field

Atmospheric transmittance η_{at} pertains to the reduction in energy due to attenuation when solar radiation travels through the atmosphere. When sunlight bounces off the heliostat and moves towards the receiver, it encounters obstacles like reflection, absorption, and scattering by nearby air or dust particles, hindering its optimal delivery to the absorber surface. The degree of transmission is related to the position of the sun, local altitude, and atmospheric conditions which influence absorption rates [13]. The value of atmospheric transmittance η_{at} is associated with the distance of reflection, as well as local air purity, atmospheric pressure, and humidity. The formula for calculating its efficiency, applicable when the heliostat-receiver distance d_{HR} is less than or equal to 1000 meters, is as follows: $(d_{HR} \leq 1000)$:

$$\eta_{at} = 0.99321 - 0.0001176 d_{HR} + 1.97 * 10^{-8} * d_{HR}^2 \quad (7)$$

In this formula, $d_{HR}=\sqrt{x^2+y^2+(H_z-h)^2}$, the geometric significance of d_{HR} is shown in Figure 3.

From the formula (7), for a mirror field with the same number of heliostats, a dense mirror field will have a higher average atmospheric transmittance. In practice, densely packed fields can significantly reduce other efficiencies. Hence, in order to enhance the collective efficiency of the array, how to balance losses stemming from atmospheric transmittance and various efficiencies is a crucial aspect in the optimization process of heliostat arrays.

2.2.3. Cosine efficiency

As shown in Figure 4, when redirecting sunlight towards a specific target, the heliostat's surface may not always remain perpendicular to the incident light rays, instead, it could be positioned at an angle. Cosine loss is the reduction in the heliostat surface area relative to the area visible to sunlight caused by this tilt. The level of cosine efficiency is directly linked to the cosine value of the angle formed between the heliostat surface's normal direction and the incoming sunlight. The heliostat reaches its peak cosine efficiency when the heliostat, concentrator, and sun are perfectly aligned in a linear configuration. This alignment also results in the incident ray, reflected ray, and surface normal vector being collinear.

In the established heliostat coordinate system aforementioned, the collector is regarded as a point, denoted by (0, 0, H_z), let $O_A\,(x_{o,A}, y_{o,A}, z_{o,A})$ denote the center coordinates of heliostat A's mirror. Given the premise, for any heliostat, the sunlight rays incident upon its mirror surface inevitably converges towards the center of the collector. Hence:

$$x = \frac{O-O_A}{|O-O_A|} = \frac{(-x_{o,A}, -y_{o,A}, H_z - z_{o,A})}{\sqrt{x_{o,A}^2 + y_{o,A}^2 + (H_z - Z_{o,A})^2}} \quad (8)$$

Let $S_{i,s} = (x_i, y_i, z_i)$, through transformation with the coordinate system established in the preceding section, at any given time instance, the incident rays on the heliostats are determined. At a specific time point, the unit normal vector of the sunlight rays is also established.

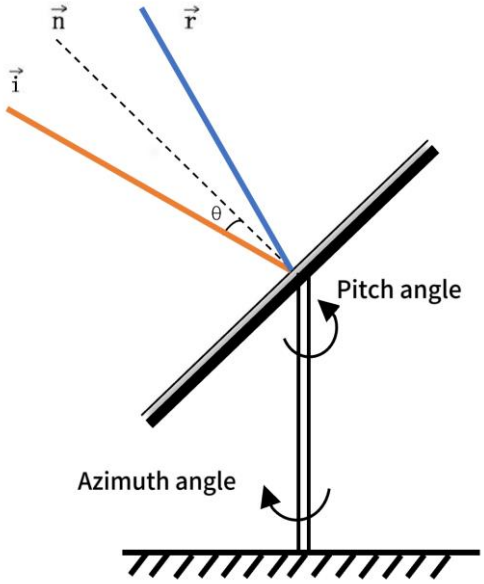

Figure 4. Cosine efficiency angle θ Schematic diagram

Hence, the computation formula (9) for $S_{i,s}$ in the coordinate system is:

$$\begin{cases} x_i = \cos(\alpha_s)\cos(\gamma_s - 90°) \\ y_i = \cos(\alpha_s)\sin(\gamma_s - 90°) \\ z_i = \sin(\alpha_s) \end{cases} \tag{9}$$

According to the law of light reflection, the normal vector of the mirror is coplanar with the incident and reflected normal vectors and bisects the angle between the incident ray and the reflected ray. Therefore, the formula (10) can be derived from the normal vector of the incident ray and the normal vector of the reflected ray:

$$S_{n,A} = \frac{S_{r,A} - S_{i,s}}{|S_{r,A} - S_{i,s}|} \tag{10}$$

Furthermore, the formula (11) can be obtained:

$$\begin{cases} tan(\theta_z) = \dfrac{sin(\alpha_s)m + h}{\sqrt{x_{o,A}^2 + y_{o,A}^2 + m^2 cos(\alpha_s)^2 - 2cos(\alpha_s)m(x_{o,A}sin(\gamma_s) - y_{o,A}cos(\alpha_s))}} \\ sin(\theta_s) = \dfrac{x_{o,A} - cos(\alpha_s)sin(\gamma_s)m}{\sqrt{x_{o,A}^2 + y_{o,A}^2 + m^2 cos(\alpha_s)^2 - 2cos(\alpha_s)m(x_{o,A}sin(\gamma_s) - y_{o,A}cos(\alpha_s))}} \end{cases} \tag{11}$$

In this formula, $x = \sqrt{x_{o,A}^2 + y_{o,A}^2 + {h_0}^2}$.

2.2.4. Shadow occlusion efficiency

In this paper, the shadowing losses due to the absorption tower obstructing the heliostats and the mutual shading among the heliostats themselves will be considered. The computational idea of this paper is shown in Figure 5.

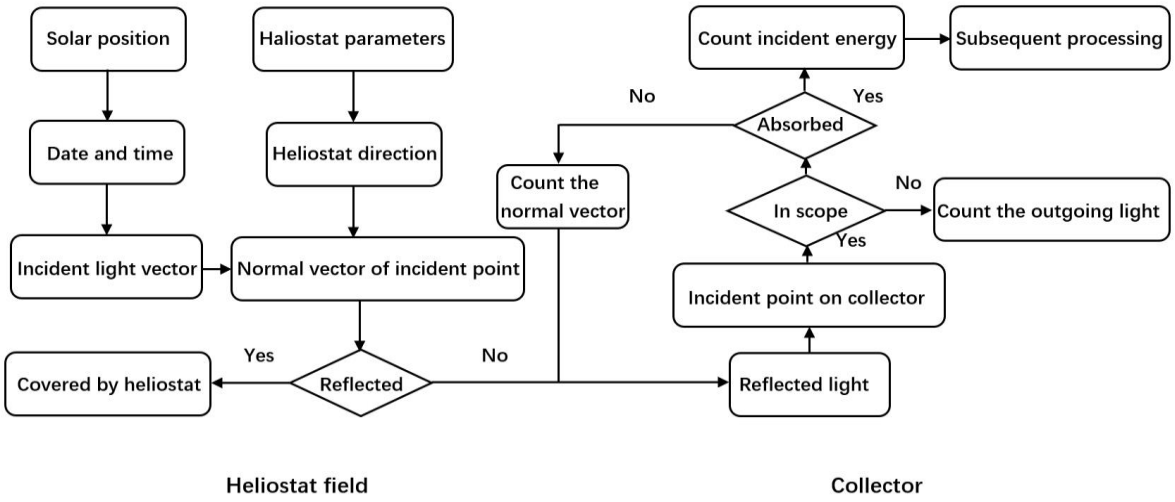

Figure 5. Flowchart for calculating shadow occlusion efficiency

The obstruction of heliostats by the absorption tower is influenced by the variation in the solar elevation angle throughout the day. At 9:00 AM and 3:00 PM, when the solar elevation angles are at their minimum, the shadow of the absorption tower is longest, resulting in the maximum shading loss to the heliostats. The method for calculating the area of the shadow cast by the absorption tower is as follows:

$$S = l^2 * \frac{|S_{r,A_1} - S_{i,s}|}{|S_{r,A_2} - S_{i,s}|} * \frac{|(S_{r,A_1} - S_{i,s})|}{|(S_{r,A_2} - S_{i,s})|} \tag{12}$$

$$S = d(H_z tan\alpha_s - 100) \tag{13}$$

Where d is the diameter of the absorption tower, H_z is the height of the absorption tower, α_s is the solar altitude angle.

At 9:00 AM, computations (12) (13) demonstrate that the shadowed area is smaller than one-thousandth of the entire reflective surface area within the heliostat field, thus can be deemed insignificant.

Mutual occlusion between heliostats. The method to determine whether there is shadow occlusion loss between the sun cones shining on the heliostat is to project another heliostat along the direction of the incident light towards the plane where the heliostat is located, obtaining its projected quadrilateral. If the tracking point on the heliostat falls within the projected quadrilateral, then the beam of tracking light has shadow occlusion loss and cannot be reflected to the collector; On the contrary, the reflected light shines onto the collector.

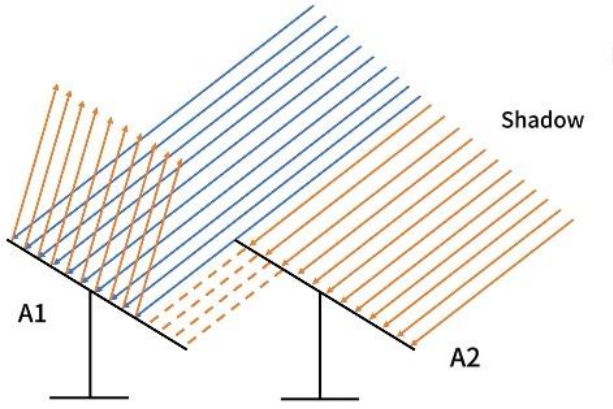

Figure 6. Schematic diagram of occlusion between heliostats

As shown in the figure 6, a part of the sun cone reflected by heliostat A_1 is blocked by heliostat A_2, That is, the projection of heliostat A_2 on the plane where A_1 is located in the direction of incident sunlight overlaps with A_1.

In the coordinate system of the heliostat field, the plane where heliostat A_1 is located is determined by its center point coordinates (x_1, y_1, z_1) and the unit normal vector $n_1 = \frac{S_{r,A_1} - S_{i,s}}{|S_{r,A_1} - S_{i,s}|}$. Similarly, there are the center point coordinates of heliostat A_2 (x_2, y_2, z_2) and the unit normal vector $n_2 = \frac{S_{r,A_2} - S_{i,s}}{|S_{r,A_2} - S_{i,s}|}$.

The unit vector expression for the direction of solar incidence $S_{i,s} = (x_i, y_i, z_i)$, then the shadow projection area of A_2 on the plane where A_1 is located is

$$S_T = l^2 \frac{\left|S_{r,A_1} - S_{i,s}\right|}{\left|S_{r,A_2} - S_{i,s}\right|} \frac{\left|(S_{r,A_1} - S_{i,s}) S_{i,s}\right|}{\left|(S_{r,A_2} - S_{i,s}) S_{i,s}\right|} \tag{14}$$

The shadow occlusion loss refers to the part of the shadow area within the A_1 mirror range, that is, any point in the loss part is less than or equal to half of the edge length between the two central axes of the fixed sun mirror and the two planes perpendicular to the plane. The calculation method for this constraint condition is as follows:

the mirror normal vector passing through the center point of A_1 is

$$S_0 = \frac{S_{r,A} - S_{i,s}}{|S_{r,A} - S_{i,s}|} \tag{15}$$

One of the unit vectors (x_a, y_a, z_a) in the direction of the central axis is

$$S_1 = \frac{S_{r,A} + S_{i,s}}{|S_{r,A} + S_{i,s}|} \tag{16}$$

The equation for the vertical plane passing through the line can be abbreviated as

$$x_a x + y_a y + z_a z + D_a = 0 \tag{17}$$

Calculating the unit vector (x_b, y_b, z_b) in the direction of the other central axis is $S_0 \times S_1$

The equation for the vertical plane passing through this line can be abbreviated as

$$x_b x + y_b y + z_b z + D_b = 0 \tag{18}$$

Therefore, the constraint conditions are:

$$\begin{cases} \frac{|x_a x + y_a y + z_a z + D_a|}{\sqrt{x_a{}^2 + y_a{}^2 + z_a{}^2}} \leq \frac{l}{2} \\ \frac{|x_b x + y_b y + z_b z + D_b|}{\sqrt{x_b{}^2 + y_b{}^2 + z_b{}^2}} \leq \frac{l}{2} \end{cases} \tag{19}$$

Where l is the side length of heliostat A.

Therefore, the shadow projection area under the constraint conditions is the calculated shadow occlusion area, and the ratio of the total shadow occlusion area to the total area of the heliostat is the shadow loss.

2.2.5. Interception efficiency of heat absorber

The interception efficiency is the efficiency of the solar energy received by the heat absorber after deducting the loss of solar energy reflected from the heliostat because it does not reach the surface of

the absorber and overflows into the outside atmosphere. Interception efficiency is related to the mirror surface error, tracking error and so on. The calculation formula is:

$$\eta_{trunc} = \frac{\textit{The energy received by heat absorber}}{\textit{Energy of mirror total reflection - energy lost in shadow occlusion}} \tag{20}$$

To simplify the assessment of whether the beam is fully projected onto the solar collector, the absorber surface of the collector will be regarded as a cylindrical unfolded surface in this paper, where the beam projected onto the absorber surface appears circular. The above model does not consider the divergence of sunlight, but rather treats it as parallel light with no angle. Nonetheless, during the evaluation of the interception efficiency of the solar collector, the incident sunlight has a small angle, referred to as the solar incidence angle. As illustrated in Figure 7, each point on the heliostat mirror receives sunlight in the form of a conical beam.

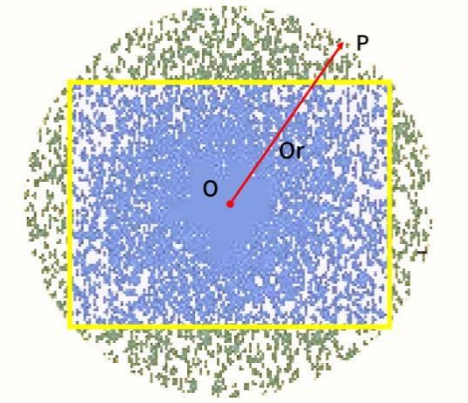

Figure 7. Schematic diagram of single beam cone cross-section using Monte Carlo method

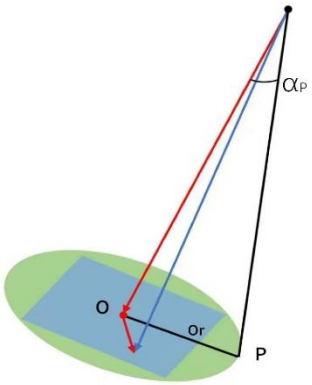

Figure 8. Schematic diagram of incident solar cone

To simulate the distribution of energy flux density resulting from the reflection of sunlight on the surface of a solar collector, the Monte Carlo method [14], a random simulation method will be adopted in this paper, and its application to radiation heat transfer calculation is the Monte Carlo ray tracing method.

Here, Monte Carlo method will be used by evenly distributing points on the heliostat surface, meshing the absorber surface and dividing the reflected light into different grids, then the number of lights in each grid of the collector receiving surface will be obtained in this paper. The more points are randomly scattered, the more realistic the simulation results will be.

In a circular beam of sunlight projected onto the receiving surface, the distribution of solar radiation energy is non-uniform at different positions within the beam. As shown in Figure 8, the primary reflection point, denoted as point O, exhibits the highest energy level, then the energy gradually decreasing to zero around it. The formula (21) (22) for Solar Disk Energy Flux Distribution will be used in this paper to represent the energy distribution of the solar disk:

$$S_\alpha = \begin{cases} S_0\left[1-\lambda\left(\frac{\alpha}{\alpha_p}\right)^4\right], \alpha < \alpha_P \\ 0, \alpha > \alpha_P \end{cases} \tag{21}$$

$$S_0 = \frac{DNI*dA}{\pi(tan\alpha_p)^2 d_{HR}^2} \tag{22}$$

Where, S_α represents the energy flux density of the light rays at an angle α with respect to the primary reflected ray. α_p denotes half of the solar diameter angle, with a value of 4.6 mrad. A represents the area of the heliostat mirror, and d_{HR} is the distance from the heliostat mirror to the image plane along the direction of the primary reflected ray.

According to equation (8), dividing α_p into several parts evenly, employing the roulette wheel selection method to randomly choose angles, and using a large number of rays to simulate the solar energy disk. The energy flux distribution of the solar disk is non-uniform. Smaller solar angles correspond to more rays, representing stronger energy. Conversely, larger angles result in fewer rays and weaker energy. When the angle exceeds α_p, the energy is zero.

3. Results

According to the formula (6) for calculating the efficiency of the heliostat field, the mean values have been obtained in Table.1. and Table.2.

Table 1. Mean optical efficiency and output thermal power on the 21st day of each month

Date	Mean optical efficiency	Mean cosine efficiency	Mean Shadow Occlusion Efficiency	Mean truncation efficiency	Mean output thermal power per unit area mirror (kW/m^2)
1.21	0.4223	0.5732	0.8353	0.8640	0.38146707
2.21	0.4111	0.5736	0.8381	0.8539	0.4137119
3.21	0.4018	0.5751	0.8412	0.8422	0.4259245
4.21	0.4173	0.5789	0.8493	0.8686	0.4349198
5.21	0.4342	0.5847	0.8532	0.8978	0.4454207
6.21	0.4500	0.5960	0.8587	0.9222	0.4447984
7.21	0.4698	0.6005	0.8565	0.8999	0.4448868
8.21	0.4574	0.5950	0.8587	0.9029	0.4404183
9.21	0.4306	0.5852	0.8356	0.8804	0.4287072
10.21	0.4315	0.5787	0.8297	0.8699	0.4035934
11.21	0.4114	0.5750	0.8157	0.8610	0.3800498
12.21	0.3937	0.5736	0.8276	0.8123	0.3654256

Table 2. Annual mean optical efficiency and output thermal power

Mean optical efficiency	Mean cosine efficiency	Mean Shadow Occlusion Efficiency	Mean truncation efficiency	Annual mean output thermal power	Mean output thermal power per unit area mirror (kW/m^2)
0.4276	0.5825	0.8412	0.8723	26.2	0.417

Hence, the four unique optical efficiencies demonstrate similar seasonal fluctuations throughout the annual cycle, exhibiting a rise from the spring to the summer followed by a decline from the summer to the winter. This discovery holds validity both empirically and theoretically, supported by robust evidence. For example, the mean optical efficiency reaches its peak between the months of June and August, alongside the other efficiencies, which can be attributed to the summer period in the Northern Hemisphere characterized by longer daylight hours and increased solar irradiance in comparison to the autumn and winter. These outcomes are in line with the information gathered by the Resource Discipline Innovation Platform, illustrating that, except under extreme weather conditions, the solar irradiance levels during the summer and autumn months notably exceed those observed in the spring and winter months, consequently resulting in heightened optical efficiencies.

4. Conclusions

In conclusion, an overview of a methodology aimed at constructing a mathematical model for solar heliostat fields has been provided in this paper. And also, this model has been used in this paper to examine a dataset containing information on heliostat fields, leading to the calculation of average optical efficiencies on a monthly and yearly basis for the heliostat field, along with the determination of the average thermal power generation per unit area of the reflective mirrors. The verification of the

proposed mathematical modeling approach in this manuscript is established based on the results derived from this analysis. While the exploration of employing different solvers to optimize optical efficiencies for layouts of heliostat fields has not been detailed study, it does introduce qualitative mathematical formulations that explain various attributes and features of heliostat fields. Potential avenues for future research could concentrate on refining strategies for heliostat field layouts like bio-inspired and spiral configurations, or investigating the utilization of a variety of metaheuristic algorithms for the identification of optimal layout parameters that can yield efficient optical efficiency results.

References

[1] Gao B, Liu J X, Sun H, et al. Optimization and Layout of Heliostat Field Based on Adaptive Gravitational Search Algorithm[J]. Journal of Solar Energy, 2022, 43(10):119-125.

[2] Sun P. Research on model predictive control of solar thermal power collection subsystem based on soft sensing modeling[D]. Lanzhou Jiaotong University, 2023.

[3] Nakul K, Abhishek P. A thorough review of the existing concentrated solar power technologies and various performance enhancing techniques[J].Journal of Thermal Analysis and Calorimetry,2022,147(24):14713-14737.

[4] Francia G. Un nouveau collecteur de l'energie rayonnante solaire: theorie et verifications experimentales[C]//United Nations conference on new sources of energy, Rome, 1961: 554-588.

[5] Francia G. Pilot plants of solar steam generating stations[J]. Solar Energy, 1968, 12(1):51-64.

[6] Nathanson A. A history of solar power art and design[M]. 2021.

[7] Mills D. Advances in solar thermal electricity technology[J]. Solar Energy, 2004.

[8] Hai A A, Ayman M, et al. Concentrating solar power (CSP) technologies: Status and analysis[J]. International Journal of Thermofluids,2023,18.

[9] Ibthisum M A, Muntasir M N, Ananta Z, et al. Conventional and Emerging CSP Technologies and Design Modifications: Research Status and Recent Advancements[J]. International Journal of Thermofluids,2023,20.

[10] Aboelmaaref M M, Zayed E M, Zhao J, et al. Hybrid solar desalination systems driven by parabolic trough and parabolic dish CSP technologies: Technology categorization, thermodynamic performance and economical assessment[J].Energy Conversion and Management,2020,220.

[11] Liu J X. Modeling and Simulation of Optical Efficiency and Optimization Layout of Heliostat Field in Tower-type Concentrated Solar Power Plants [D]. Lanzhou Jiaotong University, 2022.

[12] He Y L, Qiu Y, Wang, et al. Perspective of concentrating solar power[J]. Energy, 2020:117373.

[13] Zhang S Y, Zhou Z, Ren Y J, et al. Optimization Analysis of Absorption Tower Design Height for Tower-type Concentrated Solar Power Plants[J]. Northwest Hydropower, 2021, (06): 157-162.

[14] Dunn L W, Bahadori A A. Reflections on use of Monte Carlo methods[J]. Radiation Physics and Chemistry,2024,218111634-.